## Non-Reciprocal Supercurrents in a Field-Free Graphene Josephson Triode

John Chiles<sup>1†\*</sup>, Ethan G. Arnault<sup>1†</sup>, Chun-Chia Chen<sup>1</sup>, Trevyn F.Q. Larson<sup>1</sup>,

Lingfei Zhao<sup>1</sup>, Kenji Watanabe<sup>2</sup>, Takashi Taniguchi<sup>2</sup>,

François Amet<sup>3</sup>, Gleb Finkelstein<sup>1</sup>

<sup>1</sup>Department of Physics, Duke University, Durham, NC 27701, USA

<sup>2</sup>National Institute for Materials Science, Tsukuba, 305-0044, Japan

<sup>3</sup>Department of Physics and Astonomy, Appalachian State University, Boone, NC 28607, USA

<sup>†</sup> These authors contributed to this work equally

\*To whom correspondence should be addressed; E-mail: john.chiles@duke.edu

(Dated: August 1, 2024)

Abstract. Superconducting diodes are proposed non-reciprocal circuit elements that should exhibit non-dissipative transport in one direction while being resistive in the opposite direction. Multiple examples of such devices have emerged in the past couple of years, however their efficiency is typically limited, and most of them require magnetic field to function. Here we present a device which achieves efficiencies approaching 100% while operating at zero field. Our samples consist of a network of three graphene Josephson junctions linked by a common superconducting island, to which we refer as a Josephson triode. The three terminal nature of the device inherently breaks the inversion symmetry, and the control current applied to one of the contacts breaks the time-reversal symmetry. The triode's utility is demonstrated by rectifying a small (nA scale amplitude) applied square wave. We speculate that devices of this type could be realistically employed in the modern quantum circuits.

Keywords: Superconductivity, Josephson Junctions, Superconducting Diode Effect, Quantum Devices

Diodes form one of the most important building blocks in electronic circuits, since they can be used in AC-DC conversion, signal rectification, and photodetection. The utility of diodes resides in their ability to offer non-reciprocity – a low resistance to current flowing in one direction and a high resistance to current flowing in the opposite direction. While traditional diodes exploit P-N interfaces in semiconducting materials, a flurry of theoretical interest has focused on developing their superconducting analogues [1–9].

These studies have followed a decade-long explorations of non-reciprocal supercurrents [10–23] which in turn stem from pioneering work in the late 1960s to 1980s [24–28]. Superconducting devices that use such non-reciprocity have shown promise in applications ranging from three-wave mixing [29] to single flux quantum circuits [30]. However, the recent interest is driven by the search of novel materials which break both the inversion and time-reversal symmetry, thereby intrinsically enabling the superconducting diode effect (SDE). Such materials have indeed been experimentally identified and investigated, ranging from metallic films and proximitized semiconductors to van der Waals heterostructures [31– 42. While this direction offers a probe into the symmetry properties of novel materials, the resulting devices typically have limited diode efficiency, which is defined as a ratio of supercurrent in the forward and backward directions.

In the meanwhile, it has been realized that higher superconducting diode efficiency can be achieved in properly designed nanostructures in which the time-reversal symmetry is broken via trapped fluxes or an external magnetic field [43–47]. However, magnetic field is often

undesired for integrating the devices in superconducting circuits. In this work, we rectify this problem by creating superconducting diodes which can operate at zero external magnetic field and achieve efficiency approaching 100%. Our devices are based on multiterminal Josephson junctions made in graphene. In the past few years, the multiterminal junctions have been realized in a variety of materials [48–54] and have even found a foothold as a solution to technological problems [55, 56].

We utilize the developments of multiterminal Josephson junction design to eliminate the necessity of an applied magnetic field to achieve the SDE. The structure is based on three graphene Josephson junctions tied at the central superconducting island (Fig. 1a). Without applying a DC offset bias, all junctions are superconducting and the I-V curves are symmetric. By applying a dissipationless control current in one of the junctions, we break the time-reversal symmetry and tune the I-V curves of the other two junctions, achieving the SDE efficiencies approaching 100%. Our devices are further tunable by electrostatic gating, which allows us to adjust the scale of the supercurrent that can be rectified.

Our devices feature a trapezoidal superconducting island and three superconducting contacts labeled left (L), right (R) and bottom (B), Fig. 1a. (An additional sidegate approaching the island from the top does not contact the device and is not used in these measurements.) The contacts are connected to the island through 500 nm graphene channels which are etched such that none of the contacts are connected through graphene alone – all transport must occur through the central island. We have measured two devices which yielded very similar results. For consistency, we present the results for one of

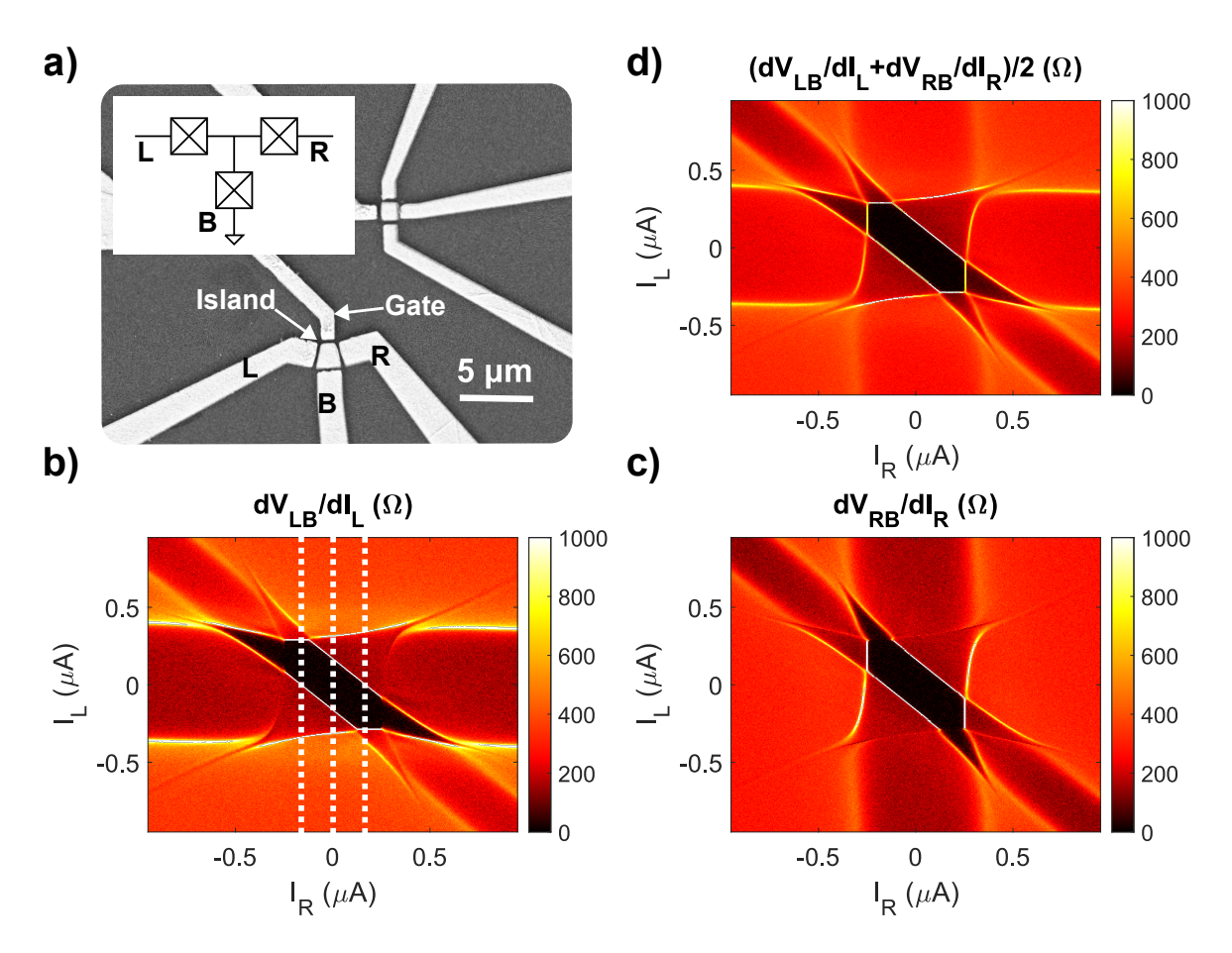


FIG. 1. a) An SEM image of the device and a schematic of the relevant Josephson network (inset). We measure the bottom one of the two similar devices, which is comprised of a superconducting island connected to three superconducting leads (L, R, B) via graphene junctions (not visible). The gate electrode approaching the island from the top is not used here. b) Map of  $\frac{dV_{LB}}{dI_L}$  with a central diamond corresponding to junctions L and B both superconducting. The dashed lines mark the locations of the I-V cuts further analyzed in Fig. 2. c) A similar map of  $\frac{dV_{RB}}{dI_R}$  with a central diamond corresponding to junctions R and B both superconducting. d) An average of the maps in (b) and (c), which emphasizes all the boundaries. The black central region demonstrates the overlap of the central diamonds in (b) and (c) – an elongated hexagon where transport through the device is dissipationless.

them, shown at the bottom of Fig. 1a.

The contacts and the island are made of sputtered molybdenum-rhenium (MoRe), which offers hightransparency Ohmic contact to graphene [57, 58]. The devices are cooled in a Leiden Cryogenics dilution refrigerator. A significant hysteresis is observed between the switching and retrapping currents at the base temperature, indicating either underdamping, or more likely electron overheating [59]. To avoid this hysteresis, the measurements are conducted in the T = 1.5 - 2 K range, as indicated in the figure captions. We have verified that all the features measured at this temperature range exhibit negligible hysteresis and can be measured by sweeping the current in any direction. DC currents  $I_L$  and  $I_R$  are applied to the left and right contacts with respect to the grounded bottom contact, and a small AC excitation is used for extracting differential resistances. To maximize the critical current, a back gate voltage of  $V_G = 20 \text{ V}$  is

applied in Figs. 1 and 2, tuning the carrier density to  $\sim 1.1-1.3\times 10^{12}~\rm cm^{-2}$ . (The Dirac point in this sample varied in the 2-5 V range between the cooldowns.) Importantly, all measurements take place at zero magnetic field.

Fig. 1b and Fig. 1c display differential resistant maps measured between the left and bottom (1b) and right and bottom (1c) contacts. As such, the prominent horizontal (1b) and vertical (1c) features correspond to the regimes where respectively the left and right junctions are superconducting. The diagonal feature common to both maps corresponds to the bottom junction being superconducting. The device's collective behavior can be gleaned from Fig. 1d where  $dV_{LB}/dI_L$  and  $dV_{RB}/dI_R$  are averaged. The distinct black region in the center of this map occurs where all three junctions are superconducting and the transport across the entire device is dissipationless.

The boundaries of the dissipationless region (an un-

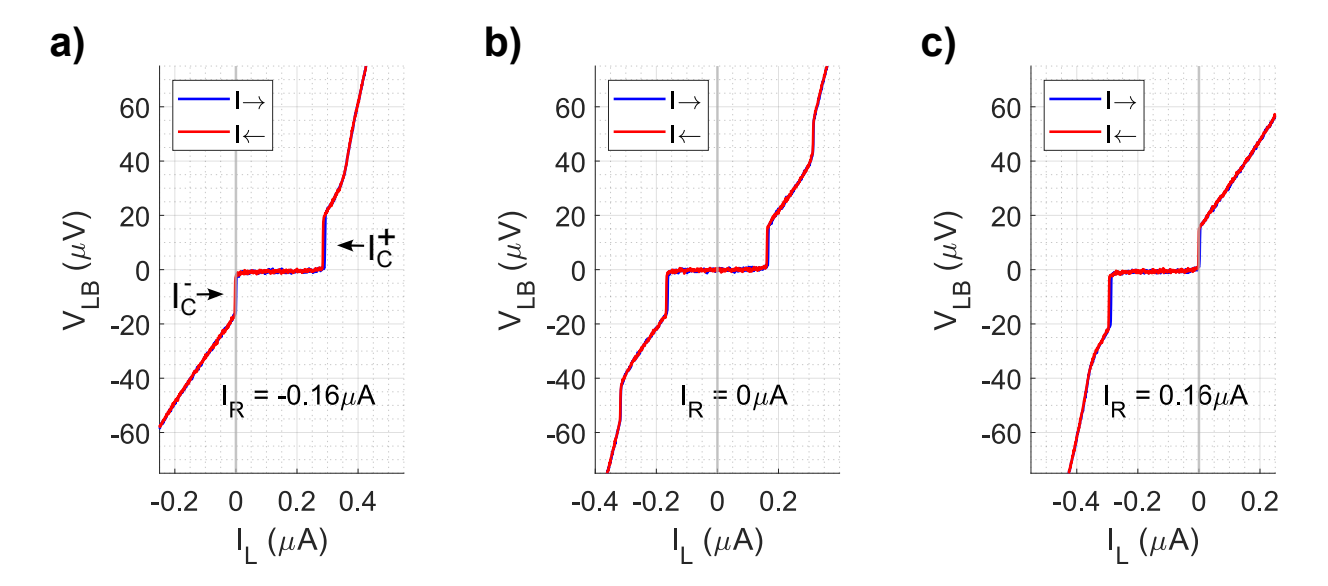


FIG. 2. I-V curves of the left junction measured at 3 values of  $I_R$ : a) -0.16  $\mu$ A, b) 0  $\mu$ A, and c) 0.16  $\mu$ A. In all cases, the control current  $I_R$  is well within the dissipationless range of the right junction. In all panels,  $I_L$  is swept back and forth, showing negligible hysteresis. In panel (b), the I-V curves are reciprocal, as expected. In (a) and (c), either  $I_c^-$  or  $I_c^+$  are approaching zero, resulting in a nearly ideal superconducting diode effect. Note that external magnetic field is equal to zero for all three panels.

even hexagon) correspond to points where at least one junction on the device switches to normal. The nonreciprocity we exploit here appears in the regions of the hexagon defined by the switching currents of two junctions. An example is the left dashed line in Fig. 1b, which cuts through the hexagonal region away from its center. As a result, the system stays dissipationless only for positive  $I_L$  and becomes dissipative at negative  $I_L$  (Fig. 2a). Note that all three junctions play a role in this this process: the bottom junction switches at  $I_L = I_c^- \approx 0$  while the left junction is responsible for the upper limit of the dissipationless range,  $I_c^+$ ; finally, it is the biasing of the right junction which establishes the required asymmetry. For zero  $I_R$ , one recovers a symmetric cross-section along the  $I_L$  direction (central white line in Fig. 1b and Fig. 2b). Finally, at the opposite value of the control current  $I_R$  (right dash line in Fig. 1b and Fig. 2c) the system stays dissipationless only at negative  $I_L \leq 0$  and the curves are reversed compared to Fig. 2a. Note that the right junction is biased below its critical current in all three cases.

Collectively, the boundaries of the hexagon enable tuning of the transport non-reciprocity between any pair of contacts by adjusting the current applied to the third contact. This leads to a diode efficiency,

$$\eta = \frac{I_c^+ + I_c^-}{I_c^+ - I_c^-},\tag{1}$$

that in practice can be tuned to approach 100%, as will be seen in Fig. 2, where we plot the I-V curves corresponding to the three cross-sections in Fig. 1b. Each set of curves is measured in both directions, showing negligible hysteresis. When  $I_R=0$  (Fig. 2b) the curves are expect-

edly symmetric, so  $I_c^+ = -I_c^-$  and  $\eta = 0$ . However, as  $I_R$  is tuned away from zero, the non-reciprocity grows and  $|\eta|$  increases until it reaches  $\approx 100\%$  at  $I_R = \pm 0.16\mu$ A.

Formally  $\eta$  can exceed unity when  $I_c^-$  becomes positive (same sign as  $I_c^+$ ). However, this regime should be avoided if we are interested in rectifying small currents. Hence we stop increasing  $|I_R|$  at the point where the high slope "knee" of the I-V curve approaches the point  $I_L=0$ . We then define  $I_c^-$  conservatively as a point at half the slope of the knee (see arrow in Fig. 2a), resulting in the  $\eta \approx 100\%$ . Finally, either positive (Fig. 2a) or negative (Fig. 2c) currents can be rectified depending on the desired operation.

To demonstrate the potential utility of the device, we apply a square wave of amplitude  $\pm$  25 nA to the left contact (Fig. 3a).  $I_R$  can then be set to produce desirable device responses: namely, at  $I_R = 0.16$  and  $-0.16\mu A$ , the negative and positive portions of the square wave are respectively rectified. Further, when  $I_R = 0$ , the device is fully superconducting for the entire square wave, as its amplitude is smaller than the critical current of the device. As a result, the entire square wave passes through the device without dissipation. Interestingly, we can change the biasing scheme to further utilize the triode's three-terminal nature. In Fig. 3b, we continue measuring  $V_{LB}$  but now use  $I_L$  as a control parameter, while applying a square wave to  $I_R$ . As a result, the voltage at the left contact,  $V_{LB}$ , switches depending on the sign of the square wave applied to the right contact.

Furthermore, the rectification demonstrated in Fig. 3(a,b) can be applied to square waves of varying amplitudes with a proper choice of control current. In Fig. 3c,  $I_R$  is kept at  $0.16\mu\text{A}$  while square waves of varying am-

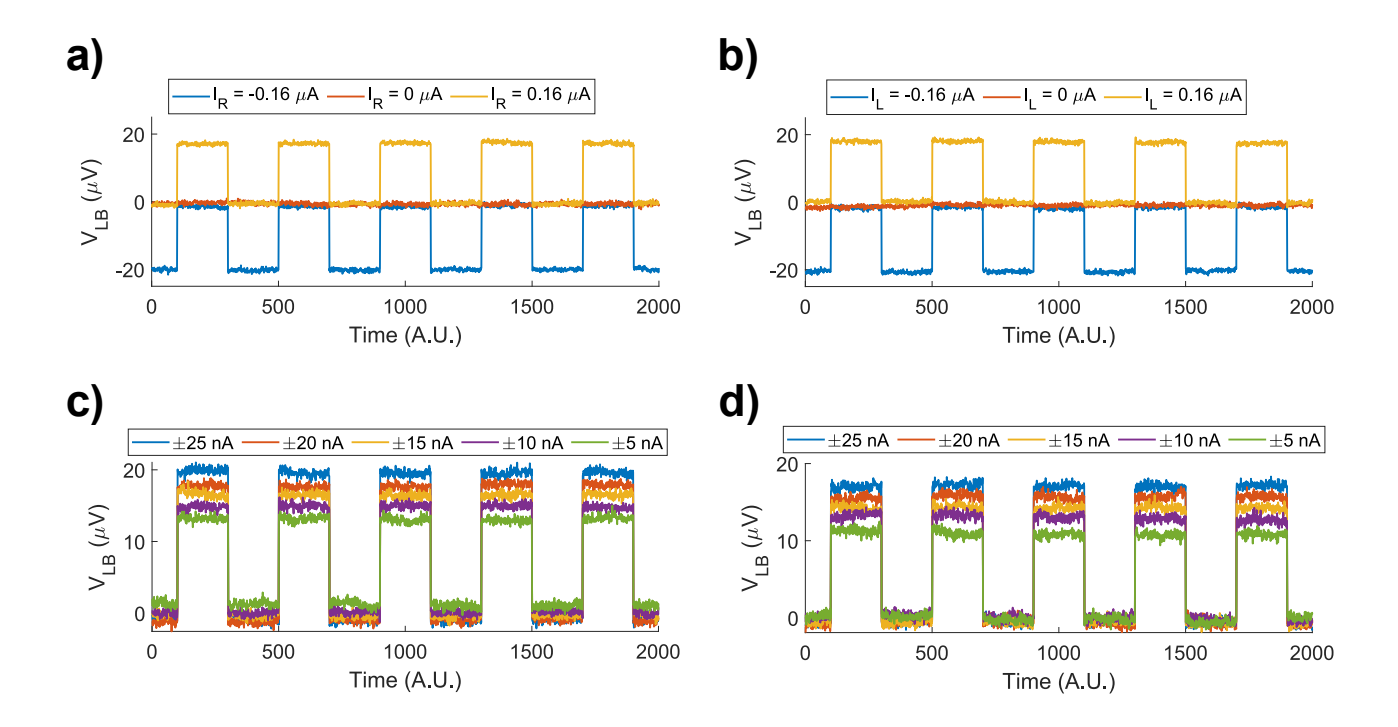


FIG. 3. a)  $V_{LB}$  measured as a square wave of a 25 nA amplitude is applied to  $I_L$ . Depending on the control current  $I_R$ , the negative and/or positive components of the square wave can be rectified (yellow and blue curve). For  $I_R = 0$ , all of the square wave lies within the dissipationless region. b) Now the square wave of amplitude 25 nA is applied to  $I_R$  instead of  $I_L$ , while still monitoring  $V_{LB}$ . Depending on the value of  $I_L$ , the negative and/or positive components of the square wave can be rectified. c) Rectification of square waves with varying amplitudes applied to  $I_L$  with  $I_R$  kept at  $0.16\mu$ A. d) Rectification of square waves with varying amplitudes applied to  $I_R$  and centered around  $I_R = 0.16\mu$ A while  $I_L = 0\mu$ A. Note that in panels (a,c) the square wave is applied to L, while in (b,d) it is applied to R.

plitudes are applied to  $I_L$ . In the measured  $V_{LB}$ , the negative portion of the square wave is rectified for waves with amplitudes as low as  $\pm$  5 nA. This is repeated in Fig. 3d, but here  $I_L$  is fixed at zero while square waves of varying amplitudes are applied to  $I_R$  centered at 0.16  $\mu$ A. Again measurements of  $V_{LB}$  demonstrate rectification of the negative half of the wave for amplitudes as low as  $\pm$ 5 nA.

Finally, Fig. 4 explores the behavior of the triode as a function of the gate voltage, which changes the critical currents by a factor of  $\sim 4$ . Pairs of maps and I-V curves are measured at the same gate and temperature: (a,d)  $V_G=4$  V and T=1.6 K, (b,e)  $V_G=10$  V and T=1.7 K, and (c,f)  $V_G=20$  V and T=2.0 K. For each value of the gate voltage, the measurement temperature is slightly adjusted to sharpen the transitions while avoiding hysteresis. Qualitatively similar behavior is observed in each column, including efficiencies approaching 100%. This feature enables a large range of working parameters in which the gate voltage and bias current could be chosen based on the experimental requirements, e.g. impedance matching and the magnitude of the rectified current.

Outside of the large non-reciprocity, the largest advantage of our design is that the time reversal symmetry is lifted without applying any sizable magnetic field. In-

deed, even small magnetic fields have been shown to induce vortices in superconducting electrodes, greatly reducing their quality factors. This would pose a problem for using magnetically controlled superconducting diodes in quantum electronic circuits. Namely, a global magnetic field on the required > 1mT scale would harm all the superconducting circuitry on the chip; applying comparable local magnetic fields would require extra wires capable of carrying the appropriately large currents. Instead, by breaking the time reversal symmetry with a current bias, the required currents are greatly reduced, producing negligible magnetic fields  $<1\mu\mathrm{T}$  which are too small to produce vortices in the diode and surrounding circuitry.

While the near perfect diode efficiency of our device is compelling, integration into quantum circuits may be fundamentally limited by the frequency cutoff and the fluctuations in the diode efficiency. The frequency cutoff is limited by the RC time constant of the device. In the present case, this can be estimated by taking the normal resistance of the graphene junction ( $\sim 500~\Omega$ ) and the capacitance of the bonding pads and leads to the silicon backgate ( $\sim 2~\mathrm{pF}$ ). Therefore, our present cutoff frequency could be as high as  $\sim 1~\mathrm{GHz}$ , indicating the promise for integrating our device into superconducting quantum circuits. Further improvements can be straight-

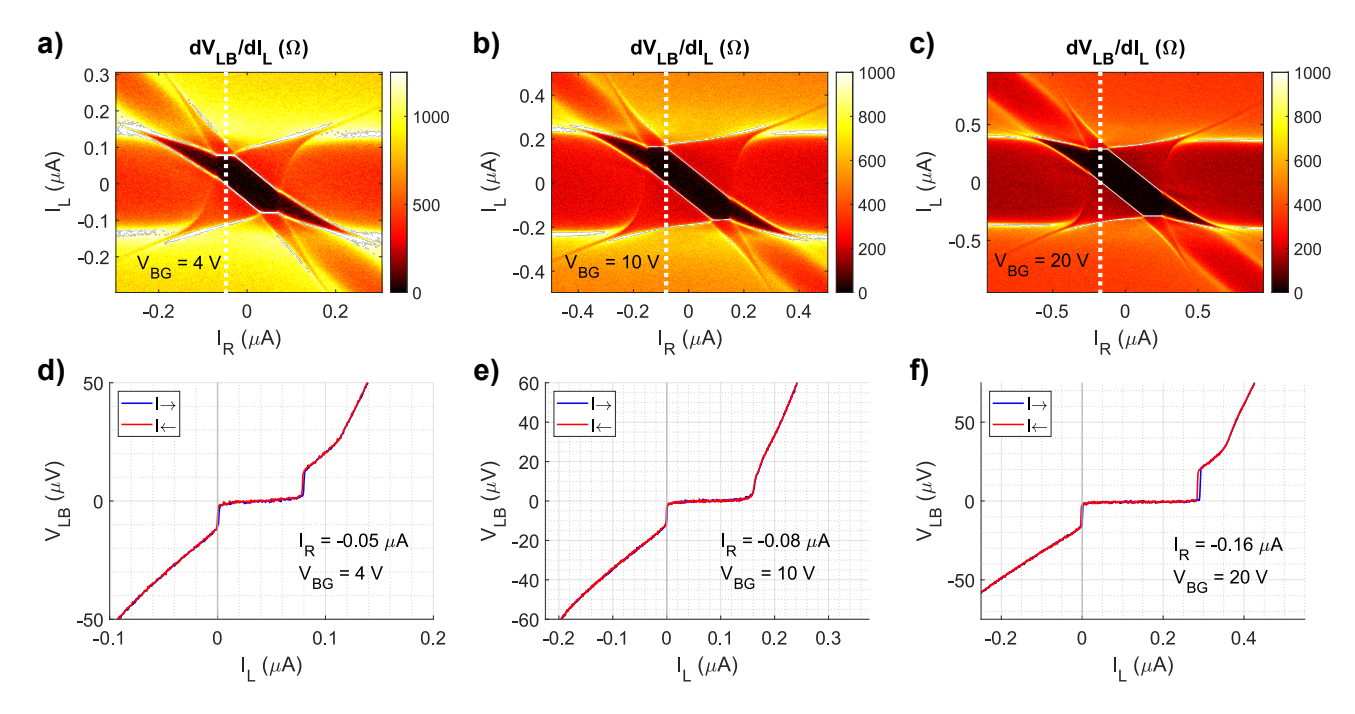


FIG. 4. (a-c) Maps of  $R_{LB} = \frac{dV_{LB}}{dI_L}$  taken at (a)  $V_G = 4$  V and T = 1.6 K, (b)  $V_G = 10$  V and T = 1.7 K, and (c)  $V_G = 20$  V and T = 2.0 K. Each map yields qualitatively similar results with expected changes of the normal-state resistance and critical currents. (d-f) I - V curves measured under the same conditions as the maps in (a-c). In each case, tuning the control current  $I_R$  enables achieving an efficiency approaching 100%. Panels (c) and (f) correspond to the data in Figures 1, 2.

forwardly made by replacing the doped  $\mathrm{Si/SiO_2}$  substrate with undoped  $\mathrm{Si}$  and moving to local gating schemes. This would greatly decrease the parasitic capacitance, especially when using the triode on-chip with the rest of the circuit.

Turning to the fluctuations of the diode efficiency, the noise of the DC control bias could be an important source. As this bias fluctuates, the diode will pick up slight changes of  $I_c^-$ , causing fluctuations of  $\eta$ . While in this measurement we have not optimized the current noise beyond reasonably acceptable levels, we have been able to limit it below  $\sim 1$  nA in the past [60]. In principle the noise in the diode could be pushed down to the quantum limit, where it is dominated by critical current fluctuations [61]. The efficiency of the triode is additionally limited by rounding of the transitions due to the operation at elevated temperature. We chose to work at higher temperature to both demonstrate the robustness of the SDE and to suppress the hysteresis of the I-V curves (see Supplementary Information). The hysteresis could be suppressed by designing the junction environment, which would in turn allow the device to operate at lower temperatures and suppress the knee.

Future implementations of our circuit geometry may also benefit by changing the junction material from graphene to tunneling junctions. Indeed, graphene allows one to tune the scale of rectified current via gate voltage (see Fig. 4), which in turn should enable better control of impedance matching and dynamic range. However, generating devices with Q-factors greater than

1000 in graphene Josephson junctions has been a challenge [62]. Meanwhile, a circuit of this device geometry implemented in tunneling junctions can maintain the high Q-factor and is more easily scalable, which can allow for rapid integration into existing quantum circuits.

Overall, our three-terminal device geometry provides field-free, highly tunable, near perfect non-reciprocities exceeding those reported in the current literature. Unlike the two-terminal devices that break time reversal symmetry (intrinsically, or via applied magnetic field), this circuit geometry should be easily scalable for rapid deployment into present-day microwave quantum systems. These benefits come at the cost of requiring the third terminal and an active biasing scheme, which may be susceptible to additional noise. However, even without optimization this platform has demonstrated rectification of very small currents.

In summary, we utilize a network of three Josephson junctions at zero magnetic field to produce a superconducting diode with efficiency approaching 100%. The device geometry – three graphene junctions connected by a common superconducting island – provides high degree of control through applied currents and gate voltage. While this device is made fairly simply in graphene, one can imagine copying the same Josephson circuit in other materials, including Al/AlO<sub>x</sub> tunnel junctions. Although in that case the gate tunability would be lost, the advantage is that the fabrication techniques are well developed and easily scalable. Further effort in this direction could quickly present opportunities for including high-efficiency

superconducting diodes in quantum circuits.

#### **METHODS**

The sample is fabricated using standard techniques in exfoliation, stacking, and electron-beam lithography. The device is etched with  $\mathrm{CHF_3O_2}$  and  $\mathrm{SF_6}$  plasma and contacts are deposited from sputtered molybdenumrhenium (MoRe).

Measurements were conducted in a Leiden Cryogenics dilution refrigerator at a base sample temperature of 60 mK. Two stage 1.5 k $\Omega/1$  nF RC filters are mounted at the mixing chamber. Current bias passed through 1 M $\Omega$  room temperature resistors, and voltage is measured with 1 nV/ $\sqrt{\rm Hz}$  ×100 homemade amplifiers. Interfacing with computer is performed with an NI USB-6363 DAQ board for both current biasing and voltage readouts.

To produce differential resistance maps as in Figure 1, the current bias on one contact is stepped in individual steps in an outer loop, while the bias on the other contact is swept quickly. From here, numerical derivatives can easily be computed to give resistance values (dV/dI). Currents are ramped in both directions (e.g.  $-1.5\mu A$  to  $1.5~\mu A$  and back to  $-1.5\mu A$ ) and all derivatives are computed (e.g.  $dV_{RB}/dI_R$  as well as  $dV_{LB}/dI_R$ ) so several maps can be produced for each measurement.

## DATA AVAILABILITY

Source data for figures (including the supplementary figures) will be made available in the public repository Zenodo prior to publication. All other data that support the plots within this paper and other findings of this study are available from the corresponding author upon reasonable request.

#### CODE AVAILABILITY

The codes used for the analysis will be made available in the public repository Zenodo prior to publication.

#### SUPPORTING INFORMATION

This material is available free of charge via the internet at https://pubs.acs.org.

 Additional data with varying temperature and magnetic field as well as mathematical modeling based on the RCSJ model

## ACKNOWLEDGEMENTS

We thank K.C. Fong for helpful discussions. Transport measurements by J.C., E.G.A., T.F.Q.L. and C.C., and data analysis by J.C., E.G.A., and G.F., were supported by Division of Materials Sciences and Engineering, Office of Basic Energy Sciences, U.S. Department of Energy, under Award No. DE-SC0002765. Sample fabrication and characterization by E.G.A. and L.Z. was supported by the NSF Award DMR-2004870. Mathematical modeling by F.A. was supported by a URC grant at Appalachian State University. K.W. and T.T. acknowledge support from JSPS KAKENHI (Grant Numbers 19H05790, 20H00354 and 21H05233). The sample fabrication was performed in part at the Duke University Shared Materials Instrumentation Facility (SMIF), a member of the North Carolina Research Triangle Nanotechnology Network (RTNN), which is supported by the National Science Foundation (Grant ECCS-1542015) as part of the National Nanotechnology Coordinated Infrastructure (NNCI).

### REFERENCES

Y. Zhang, Y. Gu, P. Li, J. Hu, and K. Jiang, General theory of josephson diodes, Phys. Rev. X 12, 041013 (2022).

<sup>[2]</sup> N. F. Q. Yuan and L. Fu, Supercurrent diode effect and finite-momentum superconductors, Proceedings of the National Academy of Sciences 119, 10.1073/pnas.2119548119 (2022).

<sup>[3]</sup> J. J. He, Y. Tanaka, and N. Nagaosa, A phenomenological theory of superconductor diodes, New Journal of Physics 24, 053014 (2022).

<sup>[4]</sup> A. Daido, Y. Ikeda, and Y. Yanase, Intrinsic superconducting diode effect, Physical Review Letters 128, 10.1103/physrevlett.128.037001 (2022).

<sup>[5]</sup> S. Ilić and F. Bergeret, Theory of the supercurrent diode effect in rashba superconductors with arbitrary disorder, Physical Review Letters 128, 10.1103/physrevlett.128.177001 (2022).

<sup>[6]</sup> K. Halterman, M. Alidoust, R. Smith, and S. Starr, Supercurrent diode effect, spin torques, and robust zero-energy peak in planar half-metallic trilayers, Physical Review B 105, 10.1103/physrevb.105.104508 (2022).

<sup>[7]</sup> H. D. Scammell, J. I. A. Li, and M. S. Scheurer, Theory of zero-field superconducting diode effect in twisted trilayer graphene, 2D Materials 9, 025027 (2022).

<sup>[8]</sup> M. Davydova, S. Prembabu, and L. Fu, Universal josephson diode effect (2022), 2201.00831, arxiv, https://arxiv.org/abs/2201.00831 (Accessed 8/15/2022).

<sup>[9]</sup> Y. Tanaka, B. Lu, and N. Nagaosa, Theory of giant diode effect in d-wave superconductor junctions on the surface of a topological insulator, Phys. Rev. B 106, 214524 (2022).

<sup>[10]</sup> A. A. Reynoso, G. Usaj, C. A. Balseiro, D. Feinberg, and M. Avignon, Anomalous josephson current in junc-

- tions with spin polarizing quantum point contacts, Physical Review Letters **101**, 10.1103/physrevlett.101.107001 (2008).
- [11] A. Zazunov, R. Egger, T. Jonckheere, and T. Martin, Anomalous josephson current through a spin-orbit coupled quantum dot, Physical Review Letters 103, 10.1103/physrevlett.103.147004 (2009).
- [12] A. A. Reynoso, G. Usaj, C. A. Balseiro, D. Feinberg, and M. Avignon, Spin-orbit-induced chirality of andreev states in josephson junctions, Physical Review B 86, 10.1103/physrevb.86.214519 (2012).
- [13] T. Yokoyama, M. Eto, and Y. V. Nazarov, Josephson current through semiconductor nanowire with spin-orbit interaction in magnetic field, Journal of the Physical Society of Japan 82, 054703 (2013).
- [14] A. Brunetti, A. Zazunov, A. Kundu, and R. Egger, Anomalous josephson current, incipient time-reversal symmetry breaking, and majorana bound states in interacting multilevel dots, Physical Review B 88, 10.1103/physrevb.88.144515 (2013).
- [15] M. A. Silaev, A. Y. Aladyshkin, M. V. Silaeva, and A. S. Aladyshkina, The diode effect induced by domain-wall superconductivity, Journal of Physics: Condensed Matter 26, 095702 (2014).
- [16] T. Yokoyama, M. Eto, and Y. V. Nazarov, Anomalous josephson effect induced by spin-orbit interaction and zeeman effect in semiconductor nanowires, Physical Review B 89, 10.1103/physrevb.89.195407 (2014).
- [17] F. Dolcini, M. Houzet, and J. S. Meyer, Topological josephson  $\phi_0$  junctions, Physical Review B **92**, 10.1103/physrevb.92.035428 (2015).
- [18] S. Hoshino, R. Wakatsuki, K. Hamamoto, and N. Nagaosa, Nonreciprocal charge transport in twodimensional noncentrosymmetric superconductors, Physical Review B 98, 10.1103/physrevb.98.054510 (2018).
- [19] R. Wakatsuki and N. Nagaosa, Nonreciprocal current in noncentrosymmetric rashba superconductors, Physical Review Letters 121, 10.1103/physrevlett.121.026601 (2018).
- [20] C.-Z. Chen, J. J. He, M. N. Ali, G.-H. Lee, K. C. Fong, and K. T. Law, Asymmetric josephson effect in inversion symmetry breaking topological materials, Physical Review B 98, 10.1103/physrevb.98.075430 (2018).
- [21] K. Misaki and N. Nagaosa, Theory of the nonreciprocal josephson effect, Physical Review B 103, 10.1103/physrevb.103.245302 (2021).
- [22] R. S. Souto, M. Leijnse, and C. Schrade, Josephson diode effect in supercurrent interferometers, Phys. Rev. Lett. 129, 267702 (2022).
- [23] Y. V. Fominov and D. S. Mikhailov, Asymmetric higherharmonic squid as a josephson diode, Phys. Rev. B 106, 134514 (2022).
- [24] A. M. Goldman and P. J. Kreisman, Meissner effect and vortex penetration in josephson junctions, Physical Review 164, 544 (1967).
- [25] T. A. Fulton, L. N. Dunkleberger, and R. C. Dynes, Quantum interference properties of double josephson junctions, Physical Review B 6, 855 (1972).
- [26] R. L. Peterson and C. A. Hamilton, Analysis of threshold curves for superconducting interferometers, Journal of Applied Physics 50, 8135 (1979).
- [27] A. Barone and G. Paternò, Physics and Applications of the Josephson Effect (Wiley, 1982).

- [28] K. K. Likharev, Dynamics of Josephson junctions and circuits (Taylor & Francis, London, England, 1986).
- [29] N. E. Frattini, U. Vool, S. Shankar, A. Narla, K. M. Sliwa, and M. H. Devoret, 3-wave mixing josephson dipole element, Applied Physics Letters 110, 222603 (2017).
- [30] V. K. Semenov, Y. A. Polyakov, and S. K. Tolpygo, New AC-powered SFQ digital circuits, IEEE Transactions on Applied Superconductivity 25, 1 (2015).
- [31] R. Wakatsuki, Y. Saito, S. Hoshino, Y. M. Itahashi, T. Ideue, M. Ezawa, Y. Iwasa, and N. Nagaosa, Nonreciprocal charge transport in noncentrosymmetric superconductors, Science Advances 3, 10.1126/sciadv.1602390 (2017).
- [32] F. Ando, Y. Miyasaka, T. Li, J. Ishizuka, T. Arakawa, Y. Shiota, T. Moriyama, Y. Yanase, and T. Ono, Observation of superconducting diode effect, Nature 584, 373 (2020).
- [33] J. Diez-Merida, A. Diez-Carlon, S. Y. Yang, Y. M. Xie, X. J. Gao, K. Watanabe, T. Taniguchi, X. Lu, K. T. Law, and D. K. Efetov, Magnetic josephson junctions and superconducting diodes in magic angle twisted bilayer graphene (2021), 2110.01067, arxiv, https://arxiv.org/abs/2110.01067 (Accessed 8/11/2022).
- [34] J. Shin, S. Son, J. Yun, G. Park, K. Zhang, Y. J. Shin, J.-G. Park, and D. Kim, Magnetic proximity-induced super-conducting diode effect and infinite magnetoresistance in van der waals heterostructure (2021), 2111.05627, arxiv, https://arxiv.org/abs/2111.05627 (Accessed 9/2/2022).
- [35] C. Baumgartner, L. Fuchs, A. Costa, S. Reinhardt, S. Gronin, G. C. Gardner, T. Lindemann, M. J. Manfra, P. E. F. Junior, D. Kochan, J. Fabian, N. Paradiso, and C. Strunk, Supercurrent rectification and magnetochiral effects in symmetric josephson junctions, Nature Nanotechnology 17, 39 (2021).
- [36] C. J. Trimble, M. T. Wei, N. F. Q. Yuan, S. S. Kalantre, P. Liu, H.-J. Han, M.-G. Han, Y. Zhu, J. J. Cha, L. Fu, and J. R. Williams, Josephson detection of time-reversal symmetry broken superconductivity in SnTe nanowires, npj Quantum Materials 6, 10.1038/s41535-021-00359-w (2021).
- [37] J.-X. Lin, P. Siriviboon, H. D. Scammell, S. Liu, D. Rhodes, K. Watanabe, T. Taniguchi, J. Hone, M. S. Scheurer, and J. Li, Zero-field superconducting diode effect in small-twist-angle trilayer graphene, Nature Physics 18, 1221 (2022).
- [38] H. Wu, Y. Wang, Y. Xu, P. K. Sivakumar, C. Pasco, U. Filippozzi, S. S. P. Parkin, Y.-J. Zeng, T. McQueen, and M. N. Ali, The field-free josephson diode in a van der waals heterostructure, Nature 604, 653 (2022).
- [39] E. Strambini, M. Spies, N. Ligato, S. Ilić, M. Rouco, C. González-Orellana, M. Ilyn, C. Rogero, F. S. Bergeret, J. S. Moodera, P. Virtanen, T. T. Heikkilä, and F. Giazotto, Superconducting spintronic tunnel diode, Nature Communications 13, 10.1038/s41467-022-29990-2 (2022).
- [40] H. Narita, J. Ishizuka, R. Kawarazaki, D. Kan, Y. Shiota, T. Moriyama, Y. Shimakawa, A. V. Ognev, A. S. Samardak, Y. Yanase, and T. Ono, Field-free superconducting diode effect in noncentrosymmetric superconductor/ferromagnet multilayers, Nature Nanotechnology 17, 823 (2022).
- [41] L. Bauriedl, C. Bäuml, L. Fuchs, C. Baumgartner, N. Paulik, J. M. Bauer, K.-Q. Lin, J. M. Lupton,

- T. Taniguchi, K. Watanabe, C. Strunk, and N. Paradiso, Supercurrent diode effect and magnetochiral anisotropy in few-layer NbSe2, Nature Communications 13, 10.1038/s41467-022-31954-5 (2022).
- [42] B. Pal, A. Chakraborty, P. K. Sivakumar, M. Davydova, A. K. Gopi, A. K. Pandeya, J. A. Krieger, Y. Zhang, M. Date, S. Ju, N. Yuan, N. B. M. Schröter, L. Fu, and S. S. P. Parkin, Josephson diode effect from cooper pair momentum in a topological semimetal, Nature Physics 10.1038/s41567-022-01699-5 (2022).
- [43] Y.-Y. Lyu, J. Jiang, Y.-L. Wang, Z.-L. Xiao, S. Dong, Q.-H. Chen, M. V. Milošević, H. Wang, R. Divan, J. E. Pearson, P. Wu, F. M. Peeters, and W.-K. Kwok, Superconducting diode effect via conformal-mapped nanoholes, Nature Communications 12, 10.1038/s41467-021-23077-0 (2021).
- [44] T. Golod and V. M. Krasnov, Demonstration of a superconducting diode-with-memory, operational at zero magnetic field with switchable nonreciprocity, Nature Communications 13, 10.1038/s41467-022-31256-w (2022).
- [45] M. Gupta, G. V. Graziano, M. Pendharkar, J. T. Dong, C. P. Dempsey, C. Palmstrøm, and V. S. Pribiag, Superconducting diode effect in a three-terminal josephson device (2022), 2206.08471, arxiv, https://arxiv.org/abs/2206.08471 (Accessed 6/30/2022).
- [46] A. Sundaresh, J. I. Väyrynen, Y. Lyanda-Geller, and L. P. Rokhinson, Diamagnetic mechanism of critical current non-reciprocity in multilayered superconductors, Nature Communications 14, 10.1038/s41467-023-36786-5 (2023).
- [47] Y. Hou, F. Nichele, H. Chi, A. Lodesani, Y. Wu, M. F. Ritter, D. Z. Haxell, M. Davydova, S. Ilić, O. Glezakou-Elbert, A. Varambally, F. S. Bergeret, A. Kamra, L. Fu, P. A. Lee, and J. S. Moodera, Ubiquitous superconducting diode effect in superconductor thin films (2022), 2205.09276, arxiv, https://arxiv.org/abs/2205.09276 (Accessed 7/28/2022).
- [48] E. Strambini, S. D'Ambrosio, F. Vischi, F. S. Bergeret, Y. V. Nazarov, and F. Giazotto, The  $\omega$ -squipt as a tool to phase-engineer josephson topological materials, Nature Nanotechnology **11**, 1055 (2016).
- [49] A. W. Draelos, M.-T. Wei, A. Seredinski, H. Li, Y. Mehta, K. Watanabe, T. Taniguchi, I. V. Borzenets, F. Amet, and G. Finkelstein, Supercurrent Flow in Multiterminal Graphene Josephson Junctions, Nano Letters 19, 1039 (2019).
- [50] G. V. Graziano, J. S. Lee, M. Pendharkar, C. J. Palm-strøm, and V. S. Pribiag, Transport studies in a gate-tunable three-terminal josephson junction, Physical Review B 101, 10.1103/physrevb.101.054510 (2020).
- [51] N. Pankratova, H. Lee, R. Kuzmin, K. Wickramasinghe, W. Mayer, J. Yuan, M. G. Vavilov, J. Shabani, and V. E. Manucharyan, Multiterminal josephson effect, Physical Review X 10, 10.1103/physrevx.10.031051 (2020).
- [52] E. G. Arnault, S. Idris, A. McConnell, L. Zhao, T. F. Larson, K. Watanabe, T. Taniguchi, G. Finkelstein, and F. Amet, Dynamical stabilization of multiplet supercurrents in multiterminal josephson junctions, Nano Letters 22, 7073 (2022).
- [53] G. V. Graziano, M. Gupta, M. Pendharkar, J. T. Dong, C. P. Dempsey, C. Palmstrøm, and V. S. Pribiag, Selective control of conductance modes in multi-terminal josephson junctions, Nature Communications 13, 10.1038/s41467-022-33682-2 (2022).

- [54] K.-F. Huang, Y. Ronen, R. Mélin, D. Feinberg, K. Watanabe, T. Taniguchi, and P. Kim, Evidence for 4e charge of cooper quartets in a biased multi-terminal graphene-based josephson junction, Nature Communications 13, 10.1038/s41467-022-30732-7 (2022).
- [55] A. Uri, A. Y. Meltzer, Y. Anahory, L. Embon, E. O. Lachman, D. Halbertal, N. HR, Y. Myasoedov, M. E. Huber, A. F. Young, and E. Zeldov, Electrically tunable multiterminal SQUID-on-tip, Nano Letters 16, 6910 (2016).
- [56] G.-H. Lee, D. K. Efetov, W. Jung, L. Ranzani, E. D. Walsh, T. A. Ohki, T. Taniguchi, K. Watanabe, P. Kim, D. Englund, and K. C. Fong, Graphene-based josephson junction microwave bolometer, Nature 586, 42 (2020).
- [57] V. E. Calado, S. Goswami, G. Nanda, M. Diez, A. R. Akhmerov, K. Watanabe, T. Taniguchi, T. M. Klapwijk, and L. M. K. Vandersypen, Ballistic Josephson junctions in edge-contacted graphene., Nature nanotechnology 10, 761 (2015).
- [58] I. V. Borzenets, F. Amet, C. T. Ke, A. W. Draelos, M. T. Wei, A. Seredinski, K. Watanabe, T. Taniguchi, Y. Bomze, M. Yamamoto, S. Tarucha, and G. Finkelstein, Ballistic graphene josephson junctions from the short to the long junction regimes, Phys. Rev. Lett. 117, 237002 (2016).
- [59] I. V. Borzenets, U. C. Coskun, H. T. Mebrahtu, Y. V. Bomze, A. I. Smirnov, and G. Finkelstein, Phonon bottle-neck in graphene-based josephson junctions at millikelvin temperatures, Phys. Rev. Lett. 111, 027001 (2013).
- [60] F. Amet, C. T. Ke, I. V. Borzenets, J. Wang, K. Watanabe, T. Taniguchi, R. S. Deacon, M. Yamamoto, Y. Bomze, S. Tarucha, and G. Finkelstein, Supercurrent in the quantum hall regime, Science 352, 966 (2016).
- [61] M. T. Haque, M. Will, M. Tomi, P. Pandey, M. Kumar, F. Schmidt, K. Watanabe, T. Taniguchi, R. Danneau, G. Steele, and P. Hakonen, Critical current fluctuations in graphene josephson junctions, Scientific Reports 11, 10.1038/s41598-021-99398-3 (2021).
- [62] F. E. Schmidt, M. D. Jenkins, K. Watanabe, T. Taniguchi, and G. A. Steele, A ballistic graphene superconducting microwave circuit, Nature Communications 9, 10.1038/s41467-018-06595-2 (2018).

# TOC GRAPHIC

